RSC Advances

ROYAL SOCIETY
OF **CHEMISTRY**

www.rsc.org/advances

One-step preparation of nitrogen doped titanium oxide / Au / reduced graphene oxide composite thin films for photocatalytic applications

A. Datcu,[a] L. Duta,[a] A. Pérez del Pino,[b] C. Logofatu,[c] C. Luculescu,[a] A. Duta,[d] D. Perniu,[d] E. György,[a,b*]

[a]National Institute for Lasers, Plasma and Radiation Physics, P. O. Box MG 36, 77125 Bucharest, Romania

[b]Instituto de Ciencia de Materiales de Barcelona, Consejo Superior de Investigaciones Científicas, (ICMAB-CSIC), Campus UAB, 08193 Bellaterra, Spain

[c]National Institute for Materials Physics, P. O. Box MG. 7, 77125 Bucharest, Romania

[d]Transilvania University of Brasov, Eroilor 29, 500036, Brasov, Romania

Abstract

TiO$_2$ and TiO$_2$ / Au / reduced graphene oxide (rGO) nanocomposite thin films were grown by ultraviolet matrix assisted pulsed laser evaporation (UV-MAPLE) in controlled oxygen or nitrogen atmospheres. An UV KrF* excimer laser (λ=248 nm, τ_{FWHM}~25 ns, ν=10 Hz) was used for the irradiation of the MAPLE targets consisting of TiO$_2$ nanoparticles (NPs) or mixtures of TiO$_2$ NPs, Au NPs, and graphene oxide (GO) platelets in aqueous solutions. The effect of Au and GO addition as well as nitrogen doping on the photocatalytic activity of the TiO$_2$ thin films was investigated. The evaluation of the photocatalytic activity was performed by photodegradation of organic methylene blue model dye pollutant under UV-visible light, "simulated sun" irradiation conditions. Our results show that the photocatalytic properties of TiO$_2$ were significantly improved by the addition of Au NPs and rGO platelets. Nitrogen inclusion into the rGO structure further contributes to the enhancement of the TiO$_2$ / Au / rGO nanocomposites photocatalytic activity.

Corresponding author, e-mail egyorgy@icmab.es, tel. +34 93 5801853 (ext. 369), fax. +34 93 5805729

1. Introduction

Titanium dioxide (TiO_2) has been widely investigated as a promising heterogeneous photocatalytic material for organic pollutants decomposition owing to its outstanding properties such as high photo-oxidative power, non-toxicity, chemical stability, and low cost [1, 2]. Air and wastewater decontamination technologies based on heterogeneous photocatalysts allow for the total mineralization of the majority of the organic pollutants (dyes, pharmaceutical and personal care produst), as well as biological pollutants (bacteria, viruses, fungi, algae, etc.) [3, 4]. The photodegradation of organic pollutant compounds is mostly conducted under UV-illumination [2]. Indeed, due to its large band gap, 3.2 eV, the optical absorption of TiO_2 is limited to the UV spectral region, which represents only about 5% of the total solar radiation. The photocatalytic activity of TiO_2 is further constrained by the fast recombination of the photo-generated charge carriers [2]. Various attempts have been made to overcome these drawbacks and to improve the efficiency of the photocatalytic processes. The investigations were focused both on the extention of the absorption region of TiO_2 to visible photons, about 42% of the total solar spectrum, as well as prevention of charge carrier recombination. The use of a large range of the solar spectrum is also mandatory for indoor applications of photocatalytic materials. Thus, cationic metal [2, 5, 6] or anionic nonmetal ion doping [2, 5-7], as well as cationic and anionic co-doping [2, 5, 6] represents possible approaches to shift the absorption edge of TiO_2 from UV towards the visible spectral region. However, the effect of dopants on the photocatalytic activity of the TiO_2 base material is still controversial. Although dopant inclusion leads to significant band gap reduction of TiO_2, the recombination rate of photo-generated charge carriers was found to increase or decrease with respect to the un-doped TiO_2 as a function of the nature as well as concentration of the dopant materials [5, 7].

To prevent electron-hole recombination reactions numerous studies have been focused on the addition of noble metal nanoparticles (NPs), Ag, Au, Pt, or Pd, which can act as scavengers for the photo-induced electrons improving this way the photocatalytic activity of TiO_2 [2, 5, 6, 8]. However, photocatalytic activity was found to be determined not only by the amount and size of the noble metal particles supported on TiO_2, but also by their distribution on the surface, properties which largely depend on the preparation conditions. Incorporation of conducting carbon nanomaterials in TiO_2 is another approach to reduce recombination rate of charge carriers and to promote electron transport. In particular, carbon nanotubes (CNTs) were found to induce charge separation [9].

2

Recent investigations showed that reduced graphene oxide (rGO) platelets, a new carbon allotrope, have positive effect on the photocatalytic decomposition of organic pollutants [10-16]. Its oxygen containing functional groups make rGO a partially insulating wide band gap semiconductor-like material and thus, a promising potential candidate for photocatalytic applications [14, 15]. To this aim, several TiO_2/rGO hybrid structures were proposed: TiO_2 nanocrystals on rGO sheets [10, 11], TiO_2/rGO composite thin films [12], or TiO_2/rGO core-shell structures [13]. Nevertheless, the mechanisms leading to the enhancement of the photocatalytic performance of composite systems containing graphene-based materials are partly unclear and controversial. Moreover, new synthesis methods have to be developed for preparing high-quality composites, with tunable chemical compositions and controlled surface morphology. As known, most conventional rGO synthesis routes do not allow for an accurate control over these properties, which in turn determine the photocatalytic activity of the composite systems. Additionally, they imply high working temperatures, of around 1000 °C or the use of toxic chemical substances [17].

In the present work we report the synthesis of TiO_2 / Au / rGO composite thin films by a single-step laser-based technique, ultraviolet matrix assisted pulsed laser evaporation (UV-MAPLE) technique. The major benefits of layered catalyst are the improved resistance to agglomeration, mechanical robustness, they can be used in continuous-flow systems and can be easyly separated from the treated water after the decomposition of organic pollutants. As concerns laser deposition methods, they have numerous advantages over conventional techniques. The chemical composition and quantity of the transferred material can be controlled through the irradiation process parameters as laser pulse energy, number of subsequent laser pulses applied for the irradiation of the targets, as well as nature and pressure of the ambient gas in the irradiation chamber [18, 19]. Reduced processing time, high reproducibility, and very low risk of cross-contamination due to the use of light as energy source stands among other relevant advantages of the laser deposition methods. MAPLE technique was applied during the last years for the immobilization of carbon nano-entities [20], SnO_2 [21] NPs, CdSe/ZnS core-shell quantum dots [22], TiO_2 nanorods [23], CNTs [24, 25], GO platelets [26], and recently TiO_2-rGO nanocomposites [27, 28]. In this work TiO_2 and Au NPs, as well as GO platelets were used as base materials for the growth of TiO_2, TiO_2 / Au / rGO, and nitrogen doped TiO_2 / Au / rGO composite thin films. We found that UV-MAPLE technique allows for the simultaneous reduction and nitrogen doping of the GO platelets. The photocatalytic performances of the prepared pristine TiO_2 and composite films were tested by the decomposition of organic methylene blue (MB, $C_{16}H_{18}ClN_3S$) model dye solutions under UV and visible light, simulated sun, irradiation conditions. Our results demonstrate that the photodegradation efficiency

3

of the synthesised materials was significantly enhanced as compared to the pure TiO_2 samples both through the addition of Au NPs and GO platelets as well as nitrogen doping.

2. Experimental

The thin film growth was performed with the aid of a MAPLE workstation consisting of a stainless steel deposition chamber and a pulsed UV KrF* (λ = 248 nm, τ_{FWHM} = 25 ns) COMPexPro 205 Lambda Physics excimer laser source. Anatase phase TiO_2 NPs with an average diameter of around 20 nm (Sigma Aldrich, 99.5%), GO sheets with about $1\mu m^2$ surface area (NanoInnova Technologies, Madrid, Spain) and Au NPs with an average diameter of around 100 nm (Sigma Aldrich, 99.5%) were used as base materials for the preparation of the MAPLE targets. The pure TiO_2 and TiO_2 / Au / GO nanocomposites thin films were prepared using dispersions in distilled water of 1 wt% TiO_2 NPs and 1 wt% TiO_2 NPs, 1 wt% Au NPs, and 5 wt% GO sheets, respectively. After thorough sonication, the dispersions were introduced immediately into a special double wall target holder and flash-frozen by circulating liquid nitrogen inside the holder walls. The targets were kept frozen during the irradiation experiments. The laser fluence was set at 400 mJ/cm^2 and the laser pulse repetition rate at 10 Hz. The laser beam incidence angle on the target surface was chosen at 45°. During the irradiation process, the laser beam scanned the target surface over a 1×1 cm^2 area at a constant velocity of 2 mm s^{-1}. A number of 10^4 subsequent laser pulses were applied for the deposition of each sample. BK7 glass plates with 1×1 cm^2 surface area were used as substrates, placed parallel to the target at a separation distance of 4 cm. During the experiments the substrates were kept at a constant temperature of 50 °C with the aid of a PID EXCEL temperature controller. Before each experiment the irradiation chamber was evacuated down to a residual pressure of 10^{-3} Pa. Comparative sets of experiments were performed in controlled O_2 or N_2 environments at pressure values in the range of (2-20) Pa.

The surface morphology of the deposited films was investigated by scanning electron microscopy (SEM) with a FEI InspectS instrument, operated at up to 30 kV acceleration voltages. To obtain information about the chemical bonds between the elements, X-ray photoelectron spectroscopy (XPS) studies were performed with the aid of a SPECS XPS spectrometer (SPECS Surface Nano Analysis GmbH, Berlin, Germany), based on Phoibos 150 electron energy analyzer operated in constant energy mode. The instrument work function was calibrated to give a binding energy of 84 eV for the Au $4f^{7/2}$ line of metallic gold. A nonmonochromatic X-ray source (MgKα line of 1253.6

eV) was used for excitation. and was run with 12.5 kV anode bias and 20 mA emission current (250W). The measurements were made in an ultrahigh vacuum at a residual pressure of around 10^{-7} Pa. A SPECS FG20 flood gun was used for the charge neutralization. High-resolution spectra were acquired over smaller ranges of 20 eV using 0.05 eV step at 10 eV pass energy. The binding energy scale of the spectra has been corrected using the C1s line. A binding energy of 284.8 eV corresponding to the C=C bonds has been assumed to this purpose. The obtained data were analyzed using SDP32 XPS software (version 7.0; XPS International, Mountain View, CA).

The photocatalytic activity of the TiO_2 and TiO_2 / Au / GO nanocomposite thin films was studied by measuring the concentration changes in time of organic MB dye in aqueous solution, under UV-VIS light – "simulated sun" (15% UV (365 nm) + 85% VIS (565 nm)) irradiation conditions. MB was applied as a model pollutant. The photodegradation reaction was carried out in a glass reactors. The samples were immersed in 20 mL solutions with 1.25×10^{-5} M (4 ppm) initial MB dye concentration (C_0) in ultrapure water, with pH = 6.8. The solutions in the reactors were continuously stirred during the photodegradation experiments. The light source consisted of two F18 W/T8 (Philips) lamps emitting in the UV spectral range of 340-400 nm with maximum emission intensity at the wavelength of 365 nm, as well as a 18 W/865 (Philips) lamp emitting in the visible spectral range between 400 and 700 nm with maximum emission intensity at the wavelength of 565 nm. All these components were placed in an aluminium housing to prevent interfering of external light in the photodegradation experiments. Prior to the initiation of the photodegradation process, adsorption experiments were carried out under dark conditions. During the adsorption and photodegradation experiments, both performed under normal atmospheric conditions, the absorbance of the solution was measured at 665 nm wavelength, which corresponds to the peak absorbance of MB in the UV–visible spectral range. The measurements were performed with the aid of a Perkin Elmer spectrophotometer. Based on the MB dye concentration–absorbance calibration curve, both the adsorption capacity and photocatalytic efficiency (η) of the samples were calculated, using the formula $\eta = (C_0-C) \times 100/C_0$, where C is the MB concentration in the aqueous solution in dark, prior to the photodegradation, or under UV-visible light irradiation during the photodegradation, measured at regular time intervals.

3. Results and discussion

The SEM image of TiO_2 thin films deposited at 2 Pa O_2 pressure is shown in Fig. 1a. As can be observed, the surface of the film is homogeneous, and consists of large spherical particles, with

sizes of hundreds on nm. The shape of the particles and their larger dimensions as compared to the initial TiO_2 NPs used for the preparation of the MAPLE targets with diameters of around 20 nm, suggest that they were formed in liquid phase through the coalescence of the initial NPs, molten under the action of the laser pulses. On the surface of the TiO_2 / Au / GO nanocomposite films (Fig. 1b,c) both the GO platelets and spherical particles can be clearly distinguished. The surface morphology of the films was found to not be significantly influenced by the pressure or nature of the ambient gas, in the studied pressure range and irradiation conditions.

In Fig. 2 we present the Ti2p XPS doublet of TiO_2 / Au / GO nanocomposite thin films obtained in O_2 (Fig. 2a) and N_2 (Fig. 2b) atmospheres. The Ti2p3/2 line of the films is centered at 459.5 eV, corresponding to the value reported for stoichiometric TiO_2 [29, 30]. This result indicates that the stoichiometry of the initial TiO_2 NPs was retained during laser processing. Moreover, the similar shape of the spectra corresponding to the films deposited in O_2 and N_2 atmosphere, and the absence of chemical shifts of the Ti2p doublet as compared to the binding energy value of stoichiometric TiO_2 reveal that no Ti-N or Ti-C bonds were formed during laser irradiation.

The Au4f doublet of the TiO_2 / Au / GO nanocomposite film deposited in O_2 atmosphere is presented in Fig. 3. The position of the Au4f7/2 and Au4f5/2 peaks coincide with the values reported in the scientific literature for metallic gold [31]. The position and area of the peaks are similar for all samples, independently on the nature or pressure of the ambient gas in the irradiation chamber.

In Fig. 4 we show the C1s spectra of a reference GO drop-cast sample, as well as TiO_2 / Au / GO nanocomposite thin film. The C1s spectrum of the reference GO drop-cast sample (Fig. 4a) was deconvoluted in five lines, corresponding to (I) C=C bonds centered at 284.8 eV binding energy and (II-V) C-O bonds of the oxygen containing functional groups situated at higher binding energies [32-34]. The C-C bonds (I) is attributed to graphite-like sp^2 C of the conjugated honeycomb lattice. The deconvoluted peaks centered at higher binding energy values are assigned to (II) C-O-C epoxy, (III) C-OH hydroxyl, (IV) C=O carbonyl, and (V) O-C=O carboxyl groups, respectively [32-34].

As compared to the reference sample, the intensity of the lines situated at high energy side of the C1s spectrum corresponding to the TiO_2 / Au / GO nanocomposite thin film obtained in 20 Pa O_2 presssure (Fig. 4 b) is significantly lower. This feature is attributed to the reduction of the number of oxygen containing functional groups after laser processing and immobilization of the GO plates. The reduction process is even more evident in case of the sample deposited in lower, 2 Pa O_2

pressure (Fig.4c). The spectrum was deconvoluted in four lines corresponding to (I) C=C bonds, (II) C-O-C epoxy, (III) C-OH hydroxyl, as well as (IV) C=O carbonyl groups, respectively [32-34]. Even though the position of the lines (II-IV) is very similar in both C1s spectra, their intensity is much reduced in case of the sample deposited in 2 Pa O_2 as compared to that obtained in 20 Pa O_2 atmosphere. Moreover, the O-C=O carboxyl groups, line (V) in the spectra of the reference GO and nanocomposite sample deposited in 20 Pa oxygen pressure, were reduced completely.

Conversely, the high binding energy side of the C1s spectrum of the samples deposited in N_2 (Fig. 4d) is broadened as compared to those deposited in O_2 atmosphere (Fig. 4c), indicating the nitrogen enclosure in the GO structure [35, 36]. As reported, the contribution of the C=N and C-N bonds is expected at the high energy side of the C1s spectra, overlapping with the peaks associated to the oxygen functional groups [35, 36]. Indeed, the intensity of the lines situated at high binding energies is significantly higher in case of the samples deposited in N_2 atmosphere (Fig. 4d) as compared to that obtained in low pressure oxygen (Fig. 4c), indicating the incorporation of nitrogen. The line (V) in Fig. 4d can be attributed to the presence of C-N bonds [35, 36], situated at binding energies similar to that corresponding to O-C=O bonds, i.e. line (V) in the spectra of the reference GO (Fig. 4a) and nanocomposite samples deposited in 20 Pa O_2 atmosphere (Fig. 4b).

For a more quantified estimation of the reduction process the A_{II}/A_I, A_{III}/A_I, and A_{IV}/A_I XPS peak area ratios were calculated (Fig. 5a). The reduction of all oxygen containing functional groups can be observed in case of TiO_2 / Au / GO nanocomposite thin film deposited in 20 Pa O_2 atmosphere as compared to the reference, non-irradiated drop-cast GO sample. The reduction process is even more relevant at low, 2 Pa oxygen pressure. The less efficient reduction in high oxygen pressure could be attributed to re-oxidation processes of the oxygen contacting functional groups during the transit of the laser ablated material from the target towards the substrate surface. Until certain extent the laser induced reduction process, leading to the formation of rGO is similar to the reported photocatalytic reduction of GO platelets in the presence of semiconductor metal oxides [37, 38]. These studies refer to UV xenon arc lamp assisted reduction of GO mixed with metal oxides and suspended in ethanol. On the other hand, the N inclusion into the GO structure is reflected by the gradual increase of the areas of the peaks situated at high binding energy side of the C1s spectra, lines II-IV, with the increase of the N_2 pressure in the irradiation chamber (Fig. 5a).

The N1s spectrum of the TiO_2/ Au / GO nanocomposite thin film deposited in 20 Pa N_2 atmosphere (Fig. 5b) was deconvoluted in three lines, assigned to nitrogen containing functional groups, which

superpose with the peaks of remaining oxygen functional groups. The lines are situated at (I) 400.4, (II) 402.2, and (III) 403.8 eV and can be attributed to (I) pyrrolic-N, (II) quaternary-N, amd (III) N-oxides of pyridinic-N, respectively [35, 36, 39, 40]. The N-doped rGO structure, showing the chemical groups identified by XPS are represented schematically in Fig. 6. Pyrrolitic-N are nitrogen atoms (NI) bounded to two carbon atoms, quaternary-N atoms (NII) replace carbon atoms in the graphene plane, called also „graphitic nitrogen", while in N-oxides of pyridinic-N (NIII) nitrogen atoms are bonded to two carbon atoms and one oxygen atom (Fig. 6). On the basis of the above discussion we can conclude that there exists no carbon or nitrogen doped TiO_2 in the laser synthesized materials. The hybrid nanostructures are formed by TiO_2, Au and nitrogen doped rGO.

The results of the photodegradation studies are presented in Fig. 7. Prior to the photodegradation experiments the adsorption-desorption equilibrium of MB on the surface of the samples was achieved after 120 min. storage of the samples in the glass reactors, in dark. The adsorption capacity of the pure TiO_2 samples was estimated to be very low, around 0.5 %, whereas that of the TiO_2 / Au / GO nanocomposite thin film was found to be slightly higher, around 2.5 %, the most probably due to the presence of the GO platelets. Indeed, rGO platelets were found to have good adsorption capabilities for organic pollutants in aqeuous solutions, through strong π–π stacking and anion–cation interactions [41]. For the photodegradation experiments the samples were placed in glass reactors containing newly prepared MB solutions. The photocatalytic efficiency of the samples deposited in oxygen atmosphere increases with the inclusion of GO platelets and Au NPs with around 170 % over the pure TiO_2 samples after the first 180 min of UV-visible light illumination (Fig. 7a). Moreover, the photocatalytic efficiency of the samples increases gradually with the increase of the nitrogen pressure as compared to that of the twin samples, deposited in oxygen atmosphere (Fig. 7a,b). Significant improvement of the photocatalytic activity of the samples was obtained, corresponding to an enhancement of around 260 % as compared to the pure TiO_2 sample, in the case of the sample deposited at high, 20 Pa N_2 pressure. These features show that photocatalytic activity of TiO_2 NPs can be controlled and enhanced with the addition of rGO platelets and Au NPs, as well as with the inclusion of nitrogen into the structure of GO platelets.

The photodegradation experiments were conducted under mixed UV and visible light, "simulated sun" irradiation conditions. The UV component, with the maximum emission intensity at the wavelength of 365 nm corresponding to 3.4 eV photon energy, greater than the band gap of TiO_2, 3.2 eV, excites electrons from the valence band to the conduction band and generates positive holes in the valence band (Eq. 1):

$$TiO_2 + hv \rightarrow TiO_2(e^- + h^+) \tag{1}$$
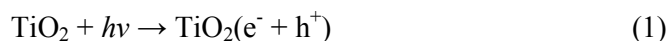
Positive holes can oxidize water molecules adsorbed at the films' surface to produce hydroxyl radicals (Eq. 2). The hydroxyl radicals can subsequently oxidize organic pollutants producing mineral salts, CO_2 and H_2O (Eq. 3):

$$H_2O + TiO_2(\ h^+) \rightarrow \ ^\bullet OH + H^+ \tag{2}$$
$$^\bullet OH + pollutant \rightarrow H_2O + CO_2 + salts \tag{3}$$

Part of the generated charge carriers can be trapped as Ti^{3+} and O^- defect sites in the TiO_2 lattice. However, the lifetime of the charge carriers is very small, they recombine rapidly, dissipating energy within a few ns [42]. rGO thanks to its electrical transport properties endowed by the π-π conjugation structure and very low amount of oxygen contaning functional groups resembling graphene, contributes to the separation of the electrons and holes, promotes the electron transport within the film, while the holes form active hydroxyl radicals in aqueous media (Eq. 2), that further oxidise the organic pollutants (Eq. 3). All these processes lead to the enhancement of the materials' photocatalytic performance [43-45]. Nitrogen inclusion further improves the electrical conductivity of rGO [46, 47], which leads to more effective separation of photo-generated charge carriers, preventing recombination, and consequently to increased photocatalytic efficiency.

Moreover, the photogenerated electrons transported across the rGO sheets react with the adsorbed O_2 on the surface to form superoxide radical anion ($O_2^{\bullet-}$) (Eq. 4) for the future photocatalytic degradation of organic pollutants (Eq. 5):

$$O_2 + rGO(e^-) \rightarrow O_2^{\bullet-} \tag{4}$$
$$O^{2\bullet-} + pollutant \rightarrow H_2O + CO_2 + salts \tag{5}$$
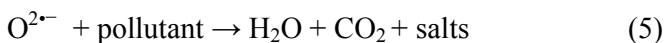
rGO platelets contribute also to the generation of electron-hole pairs both under UV and visible light irradiation (Eq. 6):

$$rGO + hv \rightarrow rGO(e^- + h^+) \tag{6}$$

Furthermore, as predicted by theoretical ab initio calculations, the visible light response of rGO/TiO_2 systhems could be attributed to the electron transferred from rGO to the conduction band

of TiO_2 [48]. The resulting photogenerated electron-hole pairs are then well-separated, leading to photocatalytic activities well beyond that of pure TiO_2 through the reduced electron-hole pair recombination [48, 49]. Moreover, deposition of noble metals on the surface of TiO_2 enhances the photocatalytic efficiency both under UV and visible light irradiation. The noble metal NPs promote interfacial charge transfer acting as electron scavengers and therefore delaying recombination of the photo-generated electron–hole pairs [2, 5, 6].

Our results demonstrate that laser techniques allow for the synthesis and immobilization of nanocomposites consisting of TiO_2, Au NPs, and rGO, as well as TiO_2, Au NPs, and N-doped rGO, in a single processing step. Through the nature and pressure of the ambient gas the GO reduction process and the formation of the nitrogen containing functional groups can be controlled, which in turn determine the functional properties of the synthesized nanocomposite materials. Moreover, recycling of the catalyst from aqueous solution subsequently to the photodegradation processes represents a critical point for their long-term use in industrial applications, due to the high cost of complicated separation process and the reduction of the photocatalyst activity during the succeeding photodecomposition processes. The laser immobilized nanocomposites can be easily isolated from the solutions after the photodegradation process and reused in subsequent degradation cycles.

Conclusion

Pure TiO_2, TiO_2 / Au / rGO, as well as nitrogen doped TiO_2 / Au / rGO nanocomposite thin films were obtained by UV-MAPLE technique. The reduction process and chemical doping of GO during laser irradiation was investigated by XPS. Oxygen functional groups containing C-O-C epoxy, C-OH hydroxyl, C=O carbonyl, and O-C=O carboxyl bonds were partially reduced during laser processing and immobilization of the GO platelets. The reduction process was determined by the ambient oxygen pressure in the laser irradiation chamber. Nitrogen was included into the rGO structure as pyrrolic-N, quaternary-N, and as N-oxides of pyridinic-N during laser irradiation in nitrogen atmosphere. The photocatalytic activity of the TiO_2 / Au / rGO nanocomposite materials synthesized in oxygen atmosphere was improved with around 170 % as compared to pure TiO_2. Moreover, the gradual incorporation of nitrogen into the rGO structure was achieved through the control of the ambient nitrogen gas pressure, leading to materials with enhanced photocatalytic efficiency, around 260 % higher as compared to pure TiO_2.

Acknowledgements

References

1. A. Fujishima and K. Honda, Electrochemical Photolysis of Water at a Semiconductor Electrode, *Nature*, 1972, **238**, 37-38.

2. J. Schneider, M. Matsuoka, M. Takeuchi, J. Zhang, Y. Horiuchi, M. Anpo, and D. W. Bahnemann, Understanding TiO_2 Photocatalysis: Mechanisms and Materials, *Chem. Rev.* 2014, **114**, 9919−9986.

3. D. Kanakaraju, B. D. Glass, and M. Oelgemoller, Titanium dioxide photocatalysis for pharmaceutical wastewater treatment, *Environ. Chem. Lett.* 2014, **12**, 27–47.

4. S. Dong, J. Feng, M. Fan, Y. Pi, L. Hu, X. Han, M. Liu, J. Sun, and J. Sun, Recent developments in heterogeneous photocatalytic water treatment using visible lightresponsive photocatalysts: a review, *RSC Adv.*, 2015, **5**, 14610–14630.

5. M. Pelaez, N. T. Nolan, S. C. Pillai, M. K. Seer, P. Falaras, A. G. Kontos, P. S. M. Dunlop, J. W. J. Hamilton, J. A. Byrne, K. O'Shea, M. H. Entezari, and D. D. Dionysiou, *Appl. Cat. B: Environ.* 2012, **125**, 331–349.

6. S. Girish Kumar and L. Gomathi Devi, Review on Modified TiO_2 Photocatalysis under UV/Visible Light: Selected Results and Related Mechanisms on Interfacial Charge Carrier Transfer Dynamics, *J. Phys. Chem. A* 2011, **115**, 13211–13241.

7. G. Sauthier, E. György, A. Figueras, R. S. Sanchez, and J. Hernando, Laser synthesis and characterization of nitrogen doped TiO_2 vertically aligned columnar array photocatalysts, *J. Phys. Chem. C* 2012, **116**, 14534−14540.

8. G. Sauthier, A. Perez del Pino, A. Figueras, and E. György, Synthesis and characterization of Ag nanoparticles and Ag loaded TiO_2 photocatalysts, *J. Am. Ceram. Soc.*, 2011, **94**, 3780–3786.

9. R. Long, Electronic Structure of Semiconducting and Metallic Tubes in TiO_2/Carbon Nanotube Heterojunctions: Density Functional Theory Calculations, *J. Phys. Chem. Lett.* 2013, **4**, 1340−1346.

10. U. L. Min, K. Zhang, W. Zhao, F. C. Zheng, Y. C. Chen, and Y. G. Zhang, Enhanced chemical interaction between TiO_2 and graphene oxide for photocatalytic decolorization of methylene blue, *Chem. Eng. J.* 2012, **193-194**, 203-210.

11. J. Zhang, Z. Xiong, and X. S. Zhao, Graphene–metal–oxide composites for the degradation of dyes under visible light irradiation, *J. Mater. Chem.* 2011, **21**, 3634-3640.

12. D. Wang, X. Li, J. Xhen, and X. Tao, Enhanced photoelectrocatalytic activity of reduced graphene oxide/TiO$_2$ composite films for dye degradation, *Chem. Eng. J.* 2012, **198-199**, 547-554.

13. H. Kim, G. Moon, D. Monllor-Satoca, Y. Park, and W. Choi, Solar Photoconversion Using Graphene/TiO$_2$ Composites: Nanographene Shell on TiO$_2$ Core versus TiO$_2$ Nanoparticles on Graphene Sheet, *J. Phys. Chem. C*, 2012, **116**, 1535-1543.

14. K. Krishnamoorthy, R. Mohan, and S. J. Kim, Graphene oxide as a photocatalytic material, *Appl. Phys. Lett*. 2011, **98**, 244101.

15. C. Su, M. Acik, K. Takai, J. Lu, S. J. Hao, Y. Zheng, P. Wu, Q. Bao, T. Enoki, and Y. J. Chabal, K. Ping Loh, *Nat. Commun*. 2012, **3**, 1298.

16. Q. Xiang, J. Yu, and M. Jaroniec, Graphene-based semiconductor photocatalysts, *Chem. Soc. Rev*. 2012, **41**, 782−796.

17. S. Pei and H. M. Cheng, The reduction of graphene oxide, *Carbon*, 2012, **50**, 3210-3228.

18. R. Eason (ed.) "Pulsed laser deposition of thin films: applications-led growth of functional materials", Wiley, Hoboken, New Jersey, 2007.

19. A. Piqué, "The matrix-assisted pulsed laser evaporation (MAPLE) process: origins and future directions", *Appl. Phys. A: Mater. Sci. Process.*, 2011, **105**, 517-528.

20. C. N. Hunter, M. Check, J. E. Bultman, and A. A. Voevodin, Development of matrix-assisted pulsed laser evaporation (MAPLE) for deposition of disperse films of carbon nanoparticles and gold/nanoparticle composite films, *Surf. Coat. Technol.*, 2008, **203**, 300-306.

21. A. P. Caricato, M. Epifani, M. Martino, F. Romano, R. Rella, A. Taurino, T. Tunno, and D. Valerini, MAPLE deposition and characterization of SnO$_2$ colloidal nanoparticle thin films, *J. Phys. D: Appl. Phys*. 2009, **42**, 095105.

22. E. György, A. Perez del Pino, J. Roqueta, B. Ballesteros, A. S. Miguel, C. D. Maycock, and A. G. Oliva, Synthesis and laser immobilization onto solid substrates of CdSe/ZnS core-shell quantum dots, *J. Phys. Chem. C*, 2011, **115,** 5210-5216.

23. M. G. Manera, A. Taurino, M. Catalano, R. Rella, A. P. Caricato, R. Buonsanti, P. D. Cozzoli, and M. Martino, Enhancement of the optically activated NO$_2$ gas sensing response of brookite TiO$_2$ nanorods/nanoparticles thin films deposited by matrix-assisted pulsed-laser evaporation, *Sens. Actuators B*, 2012, **161**, 869-879.

24. Á. Pérez del Pino, E. György, L. Cabana, B. Ballesteros, and G. Tobias, Deposition of functionalized single wall carbon nanotubes through matrix assisted pulsed laser evaporation, *Carbon*, 2012, **50**, 4450-4458.

25. E. György, Á. Pérez del Pino, J. Roqueta, B. Ballesteros, L. Cabana, and G. Tobias, Effect of laser radiation on multi-wall carbon nanotubes: study of shell structure and immobilization process, *J. Nanopart. Res*. 2013, **15**, 1852 (1-11).

26. Á. Pérez del Pino, E. György, C. Logofatu, and A. Duta, Study of the deposition of graphene oxide sheets by matrix assisted pulsed laser evaporation, *J. Phys. D: Appl. Phys*. 2013, **46**, 505309.

27. E. György, Á. Pérez del Pino, C. Logofatu, C. Cazan, and A. Duta, Simultaneous laser-induced reduction and nitrogen doping of graphene oxide in titanium oxide/graphene oxide composites, *J. Am. Ceram. Soc.,* 2014, **97**, 2718–2724.

28. S. M. O'Malley, J. Tomko, A. Pérez del Pino, C. Logofatu, and E. György, Resonant infrared and ultraviolet matrix assisted pulsed laser evaporation of titanium oxide / graphene oxide composites: a comparative study, *J. Phys. Chem. C*, 2014, **118**, 27911−27919.

29. G. Lu, S. L. Bernasek, and J. Schwartz, Oxidation of a polycrystalline titanium surface by oxygen and water, *Surf. Sci.,* 2000, **458**, 80-90.

30. M. Jobin, M. Taborelli, and P. Descouts, Structural characterization of oxidized titanium surfaces, *J. Appl. Phys*., 1995, **77,** 5149-5155.

31. N. H. Turner and A. M. Single, Determination of peak positions and areas from wide-scan XPS spectra, *Surf. Interface Anal*. 1990, **15**, 215-222.

32. D. Yang, A. Velamakanni, G. Bozoklu, S. Park, M. Stoller, R. D. Piner, S. Stankovich, I. Jung, D. A. Field, C. A. Ventrice Jr, and S. Ruoff, Chemical analysis of graphene oxide films after heat and chemical treatments by X-ray photoelectron and Micro-Raman spectroscopy, *Carbon*, 2009, **47**, 145-152.

33. Y. Matsumoto, M. Koinuma, S. Ida, S. Hayami, T. Taniguchi, K. Hatekeyama, H. Tateishi, Y. Watanabe, and S. Amano, Photoreaction of Graphene Oxide Nanosheets in Water, *J. Phys. Chem. C*, 2011, **115**, 19280-19286.

34. T. V. Khai, H. Gil, D. S. Kwak, Y. J. Kwon, H. Ham, K. B. Shim, and H. W. Kim, Significant enhancement of blue emission and electrical conductivity of N-doped graphene, *J. Mater. Chem.*, 2012, **22**, 17992- 18003.

35. D. Wei, Y. Liu, Y. Wang, H. Zhang, L. Huang, and G. Yu, Synthesis of N-Doped Graphene by Chemical Vapor Deposition and Its Electrical Properties, *Nano Letters*, 2009, **9** 1752-1758.

36. L. Sun, L. Wang, C. Tian, T. Tan, Y. Xie, K. Shi, M. Li, and H. Fu, Nitrogen-doped graphene with high nitrogen level *via* a one-step hydrothermal reaction of graphene oxide with urea for superior capacitive energy storage, *RSC Adv*. 2012, **2**, 4498-4506.

14

37. G. Williams and P. V. Kamat, Excited State Interactions Between ZnO Nanoparticles and Graphene Oxide, *Langmuir*, 2009, **25**, 13869–13873.

38. Y. H. Ng, A. Iwase, A. Kudo, and R. Amal, Reducing Graphene Oxide on a Visiblelight BiVO4 Photocatalyst for an Enhanced Photoelectrochemical Water Splitting, *J. Phys. Chem. Lett.*, 2010, **1**, 2607–2612.

39. M. Li, N. Tang, W. Ren, H. Cheng, W. Wu, and W. Zhong, *Appl. Phys. Lett*. 2012, **100**, 233112.

40. D. He, Y. Jiang, H. Lv, M. Pan, and S. Mu, *Appl. Cat. B: Envir*. 2013, **132-133**, 379-388.

41. J. N. Tiwari , K. Mahesh , N. H. Le , K. C. Kemp , R. Timilsina, R. N. Tiwari , K. S. Kim, Reduced graphene oxide-based hydrogels for the efficient capture of dye pollutants from aqueous solutions, *Carbon*, 2013, **56**, 173 – 182.

42. T. Tachikawa, M. Fujitsuka, and T. Majima, Mechanistic Insight into the TiO_2 Photocatalytic Reactions: Design of New Photocatalysts, *J. Phys. Chem. C* 2007, **111**, 5259–5275.

43. W. K. Jo and H. J. Kang, Titanium dioxide–graphene oxide composites with different ratios supported by Pyrex tube for photocatalysis of toxic aromatic vapors, *Powder Technol*. 2013, **250**, 115–121.

44. Y. Zhou, X. Zhang, Q. Zhang, F. Dong, F. Wang, and Z. Xiong, Role of graphene on the band structure and interfacial interaction of Bi_2WO_6/graphene composites with enhanced photocatalytic oxidation of NO, *J. Mater. Chem. A* 2014, **2**, 16623–16631.

45. Y. Zhang and C. Pan, TiO_2/graphene composite from thermal reaction of graphene oxide and its photocatalytic activity in visible light, *J. Mater. Sci*. 2011, **46**, 2622–2626.

46. D. H. Lee, W. J. Lee, W. J. Lee, S. O. Kim, and Y. Kim, Theory, synthesis, and oxygen reduction catalysis of Fe-Porphyrin-like carbon nanotube, *Phys. Rev. Lett*. 2011, **106**, 175502.

47. X. Yin, H. Zhang, P. Xu, J. Han, J. Li, and M. He, Simultaneous N-doping of reduced graphene oxide and TiO2 in the composite for visible light photodegradation of methylene blue with enhanced performance, *RSC Adv*., 2013, **3**, 18474.

48. A. Du, Y. H. Ng, N. J. Bell, Z. Zhu, R. Amal, and S. C. Smith, Hybrid Graphene/Titania Nanocomposite: Interface Charge Transfer, Hole Doping, and Sensitization for Visible Light Response, *J. Phys. Chem. Lett*. 2011, **2**, 894–899.

49. A. A. Ismail, R. A. Geioushy, H. Bouzid, S. A. Al-Sayari, A. A. Hajry, and D. W. Bahnemann, TiO_2 decoration of graphene layers for highly efficient photocatalyst: Impact of calcination at different gas atmosphere on photocatalytic efficiency, *Appl. Cat. B: Environm*. 2013, **129**, 62-70.

Figure caption

Fig. 1. Scanning electron microscopy images of (a) TiO_2 thin film obtained by the irradiation of a MAPLE target containing 1 wt% TiO_2 NPs in 2 Pa O_2 and (b, c) TiO_2 / Au / GO nanocomposite thin film obtained by the irradiation of a MAPLE target containing 1 wt% TiO_2 NPs, 5 wt% GO platelets, and 1 wt.% Au NPs in 2 Pa O_2 atmosphere. The experimental parameters used for the growth of the thin films were 400 mJ/cm^2 laser fluence, 10 Hz the laser pulse repetition frequency, 10^4 the number of laser pulses, and 50 °C substrate temperature.

Fig. 2. Ti2p XPS spectra of TiO_2 / Au / GO nanocomposite thin film obtained by the irradiation of a MAPLE target containing 1 wt.% TiO_2 NPs, 5 wt.% GO platelets, and 1 wt.% Au NPs in (a) 2 Pa O_2 and (b) 20 Pa N_2 atmosphere. The experimental parameters used for the growth of the thin films were 400 mJ/cm^2 laser fluence, 10 Hz the laser pulse repetition frequency, 10^4 the number of laser pulses, and 50 °C substrate temperature.

Fig. 3. Au4f XPS spectrum of TiO_2 / Au / GO nanocomposite thin film obtained by the irradiation of a MAPLE target containing 1 wt.% TiO_2 NPs, 5 wt.% GO platelets, and 1 wt.% Au NPs in 2 Pa O_2 atmosphere. The experimental parameters used for the growth of the thin films were 400 mJ/cm^2 laser fluence, 10 Hz the laser pulse repetition frequency, 10^4 the number of laser pulses, and 50 °C substrate temperature.

Fig. 4. C1s XPS spectra of (a) reference drop-cast GO sample and TiO_2 / Au / GO nanocomposite thin film obtained by the irradiation of a MAPLE target containing 1 wt.% TiO_2 NPs, 5 wt.% GO platelets, and 1 wt.% Au NPs in (b) 20 and (c) 2 Pa O_2 atmosphere as well as (d) 20 Pa N_2 atmosphere. The experimental parameters used for the growth of the thin films were 400 mJ/cm^2 laser fluence, 10 Hz the laser pulse repetition frequency, 10^4 the number of laser pulses, and 50 °C substrate temperature.

Fig. 5. (a) Relative XPS peak areas of (II) C-O-C epoxy, (III) C-OH hydroxyl, (IV) C=O carbonyl, and (V) O-C=O carboxyl bonds, normalized to the (I) C=C sp^2 component of the C1s spectra of the reference GO sample, and TiO_2 / Au / GO nanocomposite thin film obtained by the irradiation of a MAPLE target containing 1 wt.% TiO_2 NPs, 5 wt.% GO platelets, and 1 wt.% Au NPs in 20 Pa O_2, 2 Pa O_2, 2 Pa N_2, and 20 Pa N_2 atmosphere. (b) N1s XPS spectrum of TiO_2 / Au / GO nanocomposite thin film obtained by the irradiation of a MAPLE target containing 1 wt.% TiO_2 NPs, 5 wt.% GO platelets, and 1 wt.% Au NPs in 20 Pa N_2 atmosphere. The experimental parameters used for the growth of the thin films were 400 mJ/cm^2 laser fluence, 10 Hz the laser pulse repetition frequency, 10^4 the number of laser pulses, and 50 °C substrate temperature.

Fig. 6. Schematic representation of the N-doped rGO structure, showing the with chemical groups identified by XPS: (OI) C-O-C epoxy, (OII) C-OH hydroxyl, (OIII) C=O carbonyl, (OIV) O-C=O carboxyl, (NI) pyrrolic-N, (NII) quaternary-N, (NIII) N-oxides of pyridinic-N.

Fig. 7. Photocatalytic degradation rate of MB (a) after 180 min and (b) at regular reaction time intervals in the presence of TiO_2 obtained by the irradiation of a MAPLE target containing 1 wt% TiO_2 NPs and TiO_2 / Au / GO nanocomposite thin films obtained by the irradiation of a MAPLE target containing 1 wt% TiO_2 NPs, 5 wt% GO platelets, and 1 wt.% Au NPs deposited in O_2 or N_2 atmosphere and submitted to 15 % UV and 85 % visible light irradiation. The experimental parameters used for the growth of the thin films were 400 mJ/cm^2 laser fluence, 10 Hz the laser pulse repetition frequency, 10^4 the number of laser pulses, and 50 °C substrate temperature.
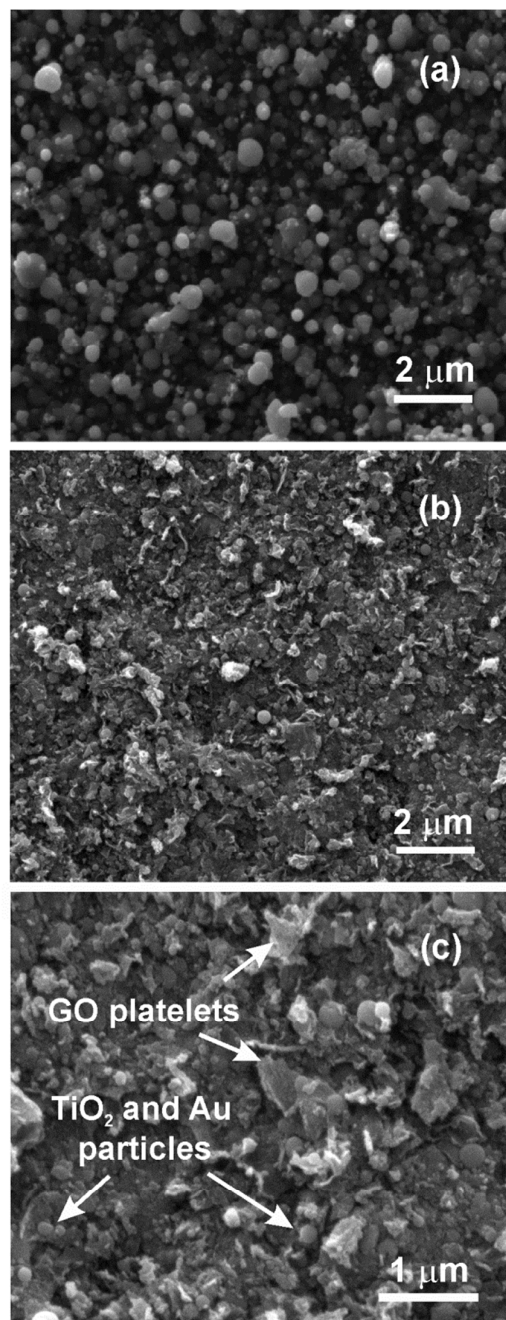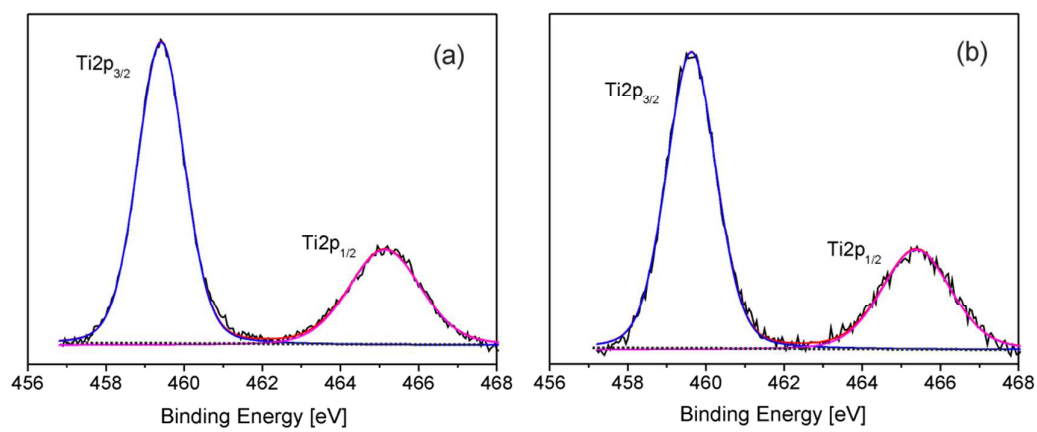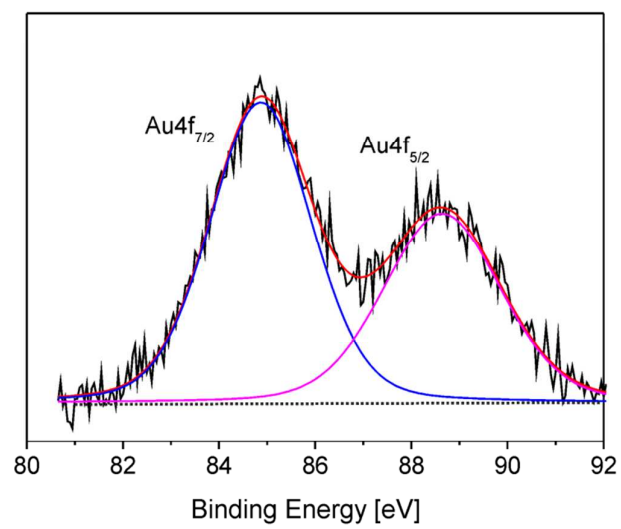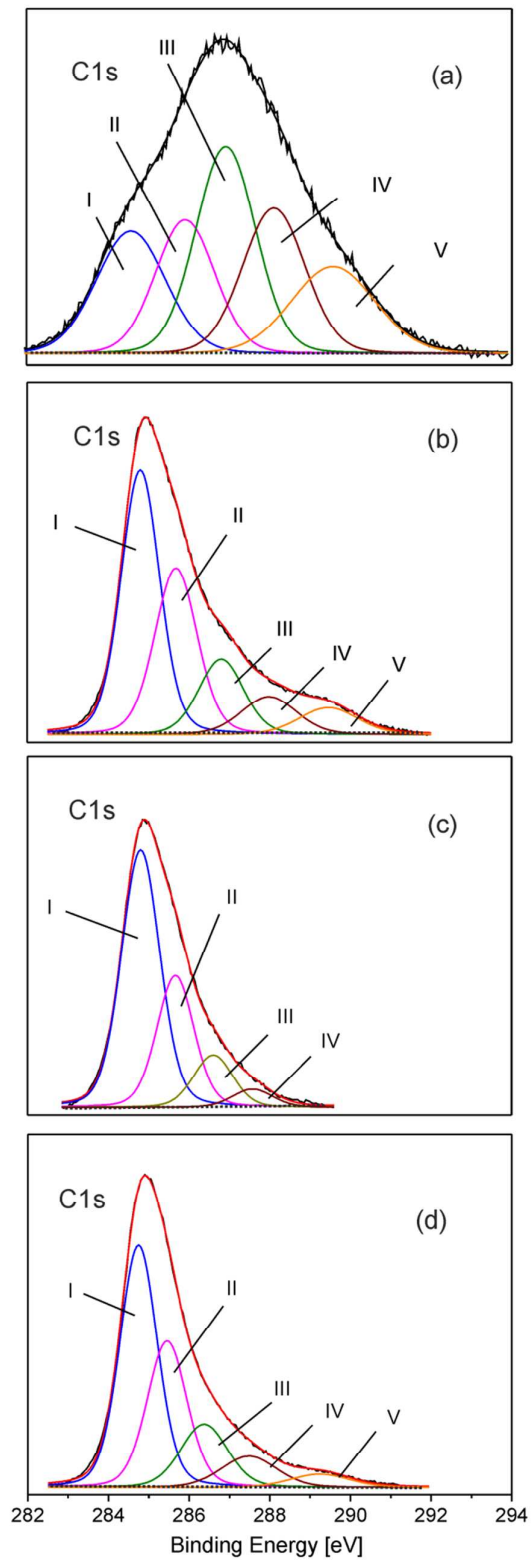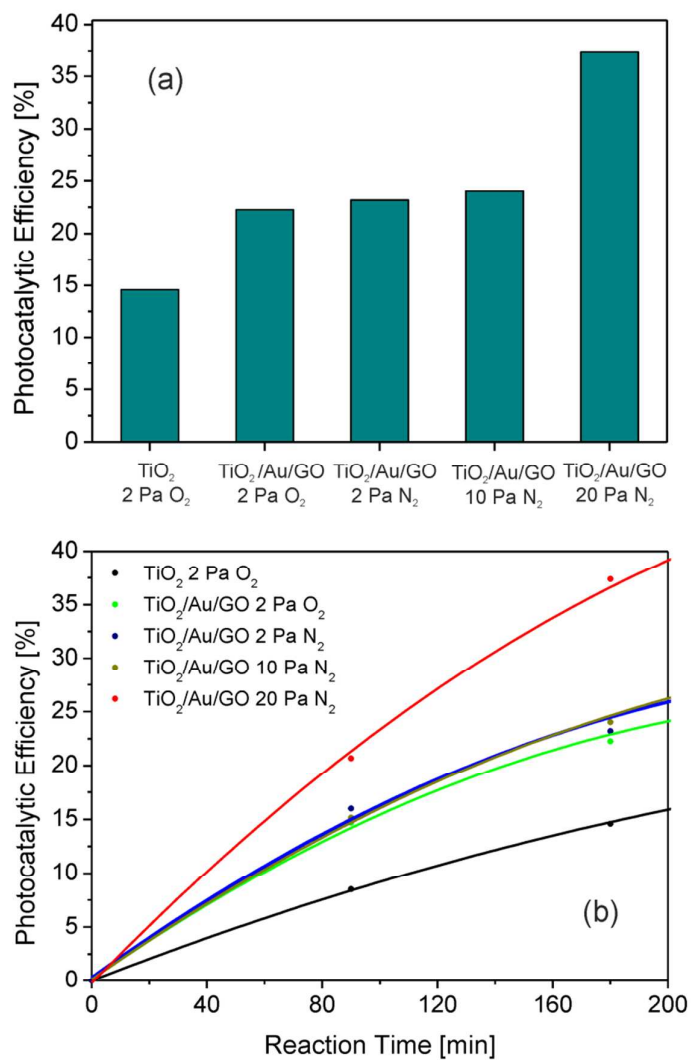
Fig. 1.

Fig. 2.

Fig. 3.

Fig. 4.

Fig. 5.

Fig. 6.

Fig. 7.